



Felfel, R.M. and Poozca, Leander and Gimeno-Fabra, Miquel and Milde, Tobias and Hildebrand, Gerhard and Ahmed, Ifty and Scotchford, Colin and Sottile, Virginie and Grant, David M. and Liefeith, Klaus (2016) In vitro degradation and mechanical properties of PLA-PCL copolymer unit cell scaffolds generated by two-photon polymerization. *Biomedical Materials*, 11 (1). 015011. ISSN 1748-605X

Access from the University of Nottingham repository:

<http://eprints.nottingham.ac.uk/34179/13/bmmaa0ca2p14%20%28002%29.pdf>

Copyright and reuse:

The Nottingham ePrints service makes this work by researchers of the University of Nottingham available open access under the following conditions.

This article is made available under the University of Nottingham End User licence and may be reused according to the conditions of the licence. For more details see: http://eprints.nottingham.ac.uk/end_user_agreement.pdf

A note on versions:

The version presented here may differ from the published version or from the version of record. If you wish to cite this item you are advised to consult the publisher's version. Please see the repository url above for details on accessing the published version and note that access may require a subscription.

For more information, please contact eprints@nottingham.ac.uk

Biomedical Materials



PAPER

In vitro degradation and mechanical properties of PLA-PCL copolymer unit cell scaffolds generated by two-photon polymerization

RECEIVED
23 June 2015

REVISED
27 November 2015

ACCEPTED FOR PUBLICATION
1 December 2015

PUBLISHED

R M Felfel^{1,4}, Leander Poocha², Miquel Gimeno-Fabra¹, Tobias Milde², Gerhard Hildebrand², Ifty Ahmed¹, Colin Scotchford¹, Virginie Sottile³, David M Grant¹ and Klaus Liefelth²

¹ Division of Materials Mechanics and Structures, Faculty of Engineering, University of Nottingham, UK

² Institute for Bioprocessing and Analytical Measurement Techniques e.V., 37308 Heilbad Heiligenstadt, Germany

³ Wolfson STEM Centre, School of Medicine, University of Nottingham, UK

⁴ Physics Department, Faculty of Science, Mansoura University, 35516, Egypt

E-mail: klaus.liefelth@iba-heiligenstadt.de and david.grant@nottingham.ac.uk

Keywords: scaffolds, stereo-lithography, photopolymerization, conversion, degradation, activation energy, compressive properties

Abstract

The manufacture of 3D scaffolds with specific controlled porous architecture, defined microstructure and an adjustable degradation profile was achieved using two-photon polymerization (TPP) with a size of $2 \times 4 \times 2 \text{ mm}^3$. Scaffolds made from poly(D,L-lactide-co- ϵ -caprolactone) copolymer with varying lactic acid (LA) and ϵ -caprolactone (CL) ratios (LC16 : 4, 18 : 2 and 9 : 1) were generated via ring-opening-polymerization and photoactivation. The reactivity was quantified using photo-DSC, yielding a double bond conversion ranging from 70% to 90%. The pore sizes for all LC scaffolds were seen 300 μm and throat sizes varied from 152 to 177 μm .

In vitro degradation was conducted at different temperatures; 37, 50 and 65 °C. Change in compressive properties immersed at 37 °C over time was also measured. Variations in thermal, degradation and mechanical properties of the LC scaffolds were related to the LA/CL ratio. Scaffold LC16 : 4 showed significantly lower glass transition temperature (T_g) (4.8 °C) in comparison with the LC 18 : 2 and 9 : 1 (see 32 °C). Rates of mass loss for the LC16 : 4 scaffolds at all temperatures were significantly lower than that for LC18 : 2 and 9 : 1. The degradation activation energies for scaffold materials ranged from 82.7 to 94.9 kJ mol^{-1} . A prediction for degradation time was applied through a correlation between long-term degradation studies at 37 °C and short-term studies at elevated temperatures (50 and 65 °C) using the half-life of mass loss (Time ($M_{1/2}$)) parameter. However, the initial compressive moduli for LC18 : 2 and 9 : 1 scaffolds were 7 to 14 times higher than LC16 : 4 (see 0.27) which was suggested to be due to its higher CL content (20%). All scaffolds showed a gradual loss in their compressive strength and modulus over time as a result of progressive mass loss over time. The manufacturing process utilized and the scaffolds produced have potential for use in tissue engineering and regenerative medicine applications.

Introduction

Biocompatible and biodegradable polymers have become commonplace for several biomedical applications such as tissue engineering scaffolds for regenerative medicine [1, 2], particulate carriers for drug delivery and targeted therapeutics as well as for bioactive coatings [2–4]. Traditional scaffold fabrication techniques have included the production of porous polymer constructs by freeze-extraction and -gelation [5], electrospinning [6], melt electrospinning [7, 8] or with hydrogels [9–12] as substrates for cell attachment.

However, complex architectures with specifically controlled micro- and macro-scale features have been difficult to achieve. Recent trends have focused on preparing multifunctional monomers which contain reactive groups (acrylates) to form cross-linked scaffolds of predefined microstructures using CAD-based manufacturing technologies [11]. Fabrication of hierarchical 3D scaffold constructs for tissue engineering, have been manufactured via 3D-printing [13], 3D-plotting [14] and stereo-lithography [15]. Resolutions of up to 50 μm have been achieved using photo-polymerization techniques for the spatial

patterning of materials in a layer-by-layer approach by stereo-lithography [16, 17]. Generation of complex structures with high resolution and without the necessity of photomasks are the major advantages of direct laser writing techniques compared to traditional lithography methods. Higher resolutions can be obtained by using two-photon absorption (TPA) where excitation wavelengths in the near-infrared (NIR) were used in combination with femtosecond pulsed lasers [18–20]. Recent works also reported possible TPA in visible light [21] or with picosecond pulses [22]. This low energy of photons makes a simultaneous TPA necessary for excitation of the photoinitiator. For sufficient photon density, femtosecond laser pulses are used. The long wavelength of the NIR allows for deeper penetration into the material and thus structuring in millimeter dimensions and a submicron resolution (figure 1(A)) [23–27]. Several research groups have been investigated the potential of 2PP for biomedical applications with biocompatible resins such as PLA [28], PCL [29], PEG [30] or the use of proteins as scaffold material [31, 32], which have the potential for clinical application [33]. The approach described here generated a scaffold for bone tissue engineering aiming to address critical size defects, offering a slow degradation rate, appropriate for bone regeneration, and provide features enabling angiogenesis and stress distribution accompanied with high loads present in bone.

The degradation rate of degradable polymers is controlled by numerous factors such as degree of crystallinity, chemical structure, molecular weight, porosity, surface/volume ratio, manufacturing methods, implantation site, applied load, degradation temperature and pH of the degradation medium [34–37]. The degradation temperature has a significant influence on the degradation of biodegradable polymers. The rate of hydrolysis is known to increase with degradation temperature which would potentially make the correlation between short-term effects at high temperature and long-term effects at physiological temperature achievable. Moreover, body temperature varies significantly between human and certain animals such as pigs and rabbits (approximately 1–3 °C higher than humans) which are commonly used as *in vivo* models [34].

The main purpose of accelerated degradation studies is to attain degradation profiles within a shorter period of time and descriptive to that obtained at standard degradation conditions [35]. Depending on the polymer and geometry, degradable devices can take up to several years for complete degradation at physiological temperature (37 °C). Therefore, validated accelerated degradation studies are an attractive research tool [38] to explore the influence of the physico-chemical factors as well as other influences such as initiators and polymer blends. Relating accelerated degradation at elevated temperatures to 37 °C allows effective fast screening rather than long term studies saving research funds and time [34].

For example a comparison of flexural strength of PLA pins degraded at 37 °C and 70 °C in saline solution

(NaCl) was performed by Claes *et al* [39]. They found that the pins completely lost their flexural strength after 18 months and 96 h of immersion in NaCl at 37 °C and 70 °C respectively. It was concluded that accelerated degradation tests can be afforded an expectation of degradation profiles in a short period of time by correlating the results of the 70 °C test with that obtained at 37 °C. Deng *et al* [40] investigated tensile properties of poly(glycolide-co-L-lactide) (PGLA) multifilament braids over time in phosphate buffered saline (PBS) solution at different temperatures (from 27.5 to 47.5 °C with 5 °C increments). A rapid loss of tensile strength was seen for specimens degraded at higher temperatures. Tensile strength of the braids decreased by ~10% after soaking in PBS for 10 d at 47.5 °C. However, 30 d were required to reach 10% loss in the strength at 37 °C. The time required to reach a given breaking strength at different temperature followed an Arrhenius equation and the activation energies calculated were 96.12 to 102.38 kJ mol⁻¹.

In the present study, porous 3D scaffolds based on methacrylated poly(D,L-lactide-co- ϵ -caprolactone) (PLCL) copolymer of different compositions and chain lengths (LC16 : 4, LC18 : 2 and LC9 : 1; numbers represent monomer units L (Lactide) and C (Caprolactone)) were manufactured via two photon polymerization technology in dimensions of 2 × 4 × 2 mm³ (see figure 1(B)). The 3D scaffold structures were based on a Schwarz Primitive (P) minimal surface derived unit cells which potentially have higher loadbearing capacities due to their strain distribution. By combining the unit cells, a scaffold of controlled pore size, porosity and dimensions was generated. *In vitro* degradation was conducted for the scaffolds at varying temperatures (37, 50 and 65 °C). The retention of compressive properties of the scaffolds was also explored during immersion and at 37 °C for 83 d. Furthermore, the influence of change in the composition and chain length of the lactide-caprolactone containing precursor material on scaffold properties (stiffness, degradation rate) was also examined.

Materials and methods

ϵ -Caprolactone (CL, Sigma-Aldrich, 97%), diethylene glycol (DEG, Sigma-Aldrich, 99%), 3,6-dimethyl-1,4-dioxane-2,5-dione (D,L-lactide, Sigma-Aldrich), methacryloyl chloride (MACL, Sigma-Aldrich, 97%), H-methoxyphenol (MEHQ, Sigma-Aldrich, 99%), stannous 2-ethylhexanoat (Sigma-Aldrich, 95%), triethylamine (TEA, Merck, 99%), Irgacure369TM (Cibachemicals) and BA740 (Organic Chemistry Department, University of Jena) as photoinitiators were used as received without further purification. Solvents were of commercial reagent grade.

Precursor synthesis

Synthesis of methacrylated random copolymers of lactic acid (LA) and ϵ -caprolactone (CL) was adapted from

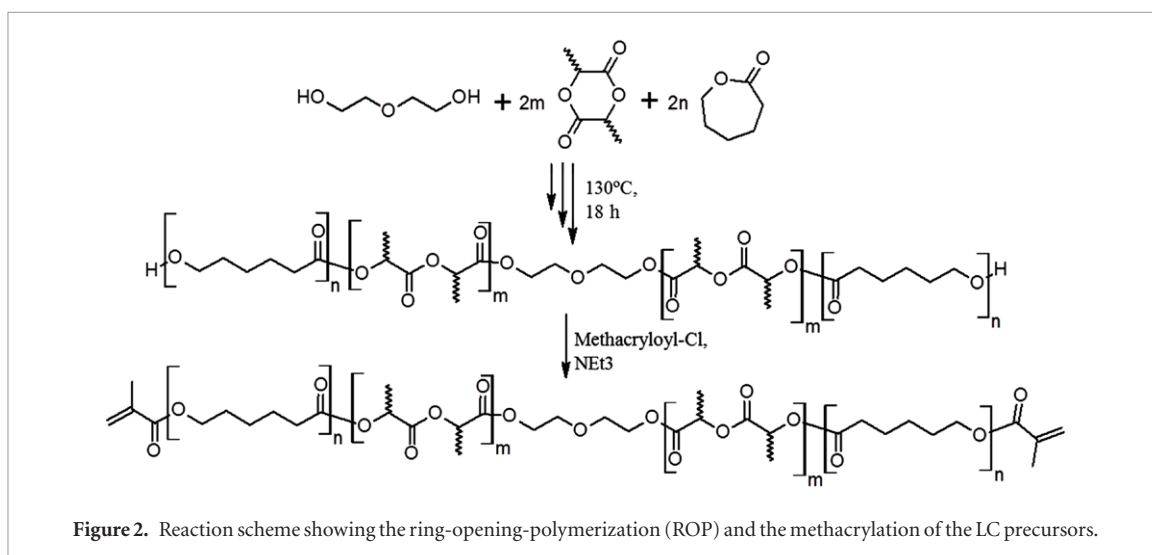
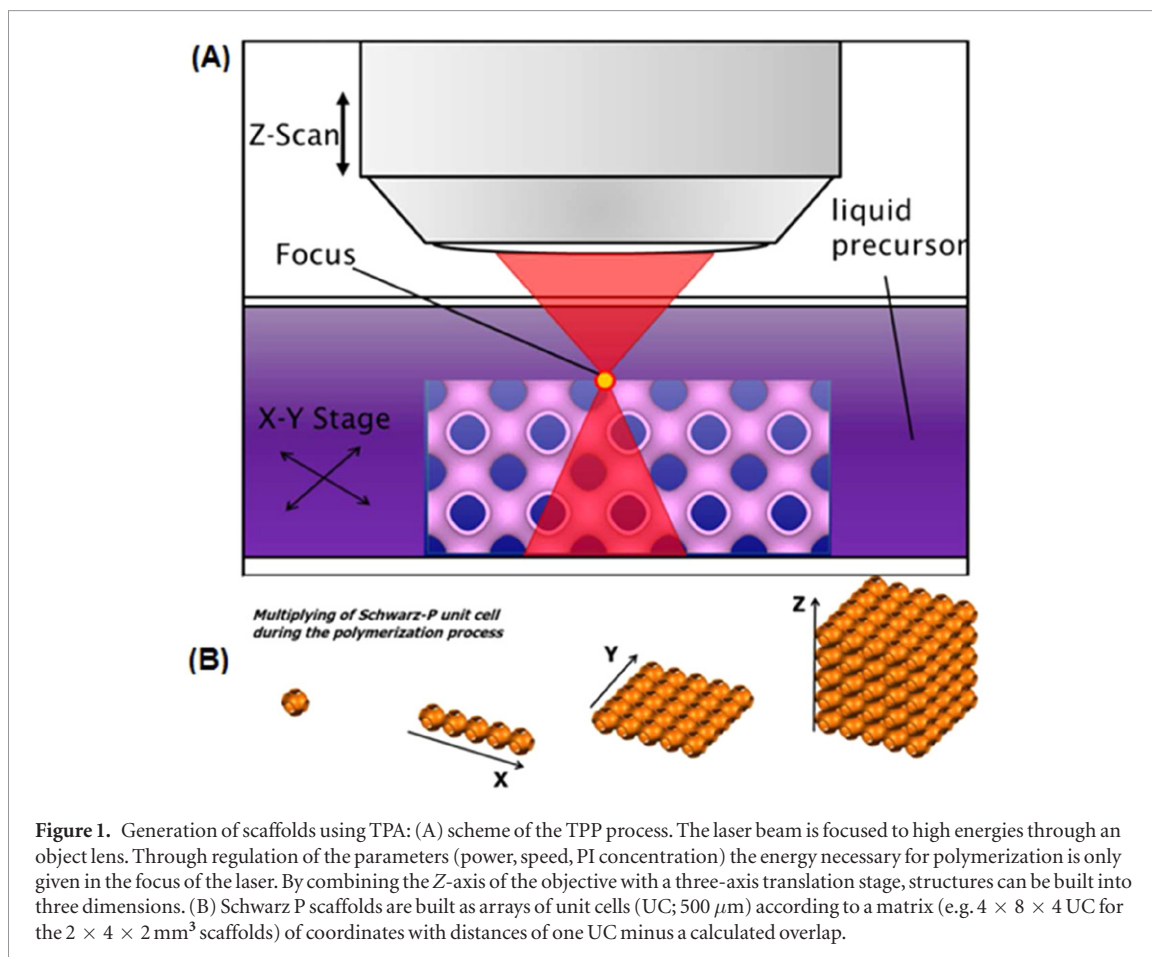


Table 1. Experimental details for LC synthesis. DEG amount remained constant.

	LA		CL		TEA		MACL	
	m [g]	n [mmol]	m [g]	n [mmol]	m [g]	n [mmol]	m [g]	n [mmol]
LC16 : 4	18.90	131.13	7.65	67.02	4.71	46.54	4.33	41.42
LC18 : 2	23.63	163.95	3.83	33.55	4.71	46.54	4.33	41.42
LC9 : 1	11.82	81.97	1.92	16.78	5.11	50.50	4.84	46.32

LA: D,L-lactide, CL: ϵ -Caprolactone, TEA: trimethylamine and MACL: methacryloyl chloride

Davis *et al* [41], but using a benzene-free purification that yields an amine free product. Figure 2 shows reaction scheme of the ring-opening-polymerization

(ROP) for the LC precursors. In brief, quantities of D,L-Lactide, ϵ -caprolactone and DEG (2.00 g, 18.85 mmol) (see table 1) were added to a 500 ml Schlenk

round bottom flask, stirred and heated to 130 °C until all lactide melted. Stannous 2-ethylhexanoate (300 μL , 0.33 mmol) was then added and reacted overnight at 130 °C under vacuum. After cooling to RT and flushing with argon, methylene chloride (100 ml) was added and the solution was cooled to 0 °C. The introduction of photoactive methacryl-groups for 2PP was achieved by the addition of TEA followed by dropwise addition of diluted MACL (in 75 ml methylene chloride). Afterwards, the flask was warmed to RT and left under continuous stirring overnight. The precipitate was then collected by filtration and the methylene chloride evaporated under reduced pressure. The resulting viscous liquid was dissolved in 50 ml of ethyl acetate, filtered again and added dropwise into 500 ml of *n*-hexane under stirring. The precipitate was then taken up in methylene chloride and washed with aqueous hydrochloric acid (3%, 2 \times 100 ml), saturated aqueous sodium bicarbonate solution (to protonate and wash off unreacted trimethylamine which is known to impair photoinitiation [42–44]) and saturated aqueous sodium chloride solution (200 ml) and then dried over anhydrous sodium sulfate. Subsequently, 300 ppm of MEHQ (300 ppm) was added to the final product.

Methacrylation degree, molecular weight and average number of LA and CL units were quantified by $^1\text{H-NMR}$ analysis. A yield of 70–75% of a colorless liquid was obtained. $^1\text{H-NMR}$ (300 MHz, CDCl_3 , d, ppm): 1.2–1.6 (m, CH_3 -LA, – CH_2 -CL), 1.8 (s, CH_3 -C(=CH $_2$)), 2.3 (m, methylene protons adjacent to carbonyl carbon in CL), 3.6 (m, DEG ether protons), 4.0–4.2 (m, CH_2 -O), 5.0 (m, LA backbone), 5.5 (s, CH_2 = C), 6.2 (s, CH_2 = C).

Photo-DSC

The photo-reactivity of LC-crosslinkers was characterised using photo-DSC (Netzsch Phoenix 204 F1, μ -sensor). In curing experiments, 2–10 mg samples containing 2% of Irgacure369TM (note BA740 could not initiate the samples curing under UV irradiation) were loaded in open aluminum crucibles and cured for 10 min at 30 °C, 50 °C and 70 °C using S2000 UV-lamp (Omni Cure). Samples were kept for 10 min at each temperature before application of UV.

The data of interest from photo-DSC measurements were the time of maximal heat production, t_{max} , measured in seconds, determined by the position of the peak maximum and the heat of polymerization, ΔH_p , measured in Joule per gram as a part of the reaction rate equation [45];

$$R_p = \frac{dH}{dt} \cdot \frac{1}{\Delta H_p \cdot m} \quad (1)$$

and determined by peak integration. Measurements of the molar heat of polymerization (J mol^{-1}) were calculated on the basis of the molecular weight and degree of methacrylation determination of NMR-analysis. The heat of the samples $\Delta H_{\text{sample}}(t)$ was calculated as follows, where 2 is the theoretical number

of methacryl groups with respect to the methacrylation degree $\%_{\text{MA}}$ multiplied with the theoretical heat of a methacryl group ΔH_{MA} (55 kJ mol^{-1}) [46], divided by the molecular weight of the sample M_{sample} .

$$\Delta H_{\text{sample}}^{\text{theo}} = \frac{2 \cdot \%_{\text{MA}} \cdot \Delta H_{\text{MA}}}{M_{\text{sample}}} \quad (2)$$

The degree of double bond conversion was then calculated with equation (3):

$$\alpha = \frac{\Delta H_{\text{sample}}^{\text{DSC}}}{\Delta H_{\text{sample}}^{\text{theo}}} \cdot 100 \quad (3)$$

TPP structuring of LC scaffolds

For processing the precursor LCs were mixed with BA740 dissolved in acetone ($0.2 \text{ mg } \mu\text{L}^{-1}$) to a final concentration of 0.2% and stirred overnight at 60 °C to ensure good distribution and evaporation of excess solvent.

The TPP apparatus (M3DL, LZH Hannover, Germany) was equipped with a femtosecond laser source with 800 nm wavelength, delivering 140 fs pulses at 80 MHz repetition rate (VISION II, Coherent, Scotland). The beam was focused by an x63 objective lens with NA 0.75 (LD-Plan-NEOFLUAR, Zeiss, Germany) into the photoresist. Structures were produced by moving the sample with a three axis nano-positioning stage according to the computer model supported by a galvanoscanner (Aerotech, USA). Writing velocities of 5 mm s^{-1} for the axis and 50 mm s^{-1} for the scanner were used. The production time for producing one sample was 96 min. The cw-Power levels of 180 mW (see 9.2 TW cm^{-2}) were used for writing, measured behind the objective.

The Schwarz P 520 μm unit cells were arrayed to the final dimension of $2 \times 4 \times 2 \text{ mm}^3$ which was limited in Z due to the objective to focus distance (approx. 2 mm). An overlay of 10 μm between two unit cells was necessary for proper structure stability. However, scaffolds with different geometries and dimensions were manufactured. Scaffolds with dimensions of $2 \times 4 \times 2 \text{ mm}^3$ were used in this study to maintain the ratio of the height to width to be 2 for compression testing specimens.

Scanning electron microscopy (SEM)

Morphology of the produced scaffolds was examined using SEM (JEOL 6400) with working distance of 20 mm and an accelerating voltage of 10 kV in secondary electron imaging mode (SE). Samples were sputter-coated with platinum for 90 s at 2.2 kV using a Polaron SC7640 coater (Quorum Technologies, UK) to obtain a coating thickness of see 15 nm. Top surfaces of the scaffolds were scanned. Size of pores and pore throats of LC scaffolds were measured using Image J 1.42 q software. Pore size was determined as average diameter of all maximal fitted spheres for each individual pore, whilst throat size represented the mean diameter of

maximal spheres inscribed at the junctions between every two pores. Aspect ratios of the pores, the ratio of minor to major axes of the pore, were also determined. A total of 20 measurements were taken and results were reported by mean values \pm standard deviation.

Sterilization of scaffolds

All the manufactured LC scaffolds were kept in a well plate and packed in Tyvek[®] sterilization pouches (Westfield Medical Ltd, UK). The samples were irradiated according to BS EN ISO 11137-2 standard [47] with a dose of 25 ± 2.5 kGy using a ⁶⁰Co gamma-ray source (Systagenix/GSS, UK). Scaffolds remained in sterilisation pouches prior to use.

Differential scanning calorimetry (DSC)

DSC analysis was performed using a DSC Q10 (TA Instrument, USA) which was calibrated using indium. Samples (~5 mg) were placed into aluminum pans and heated over a temperature range from -20 to 450 °C at a rate of 10 °C min^{-1} under nitrogen gas flow (50 ml min^{-1}). The resulting thermograms were analyzed using TA universal analysis 2000 software to determine the glass transition temperature (T_g) and decomposition temperature (T_d) of the scaffold.

Degradation study

The degradation study of the scaffolds was done according to the standard BS EN ISO 10993-13 : 2010 [48]. Scaffolds were placed individually into glass vials containing 30 ml Phosphate buffered saline (PBS) (pH = 7.4 ± 0.2) solution and maintained in ovens at 37, 50 and 65 °C. At various time points the specimens were extracted with tweezers and agitated gently to remove surplus solution before weighing. The samples were placed into empty vials and inserted within a vacuum oven (Medline Scientific, UK) at 50 °C for 60 min for drying. Afterwards, the dry weight of the scaffolds was recorded and samples were then returned to vials containing PBS.

The percentage mass change was determined using the following equation;

$$\text{Mass loss (\%)} = \left[\frac{(m - m_i)}{m_i} \right] \times 100 \quad (4)$$

where m is the mass of degraded sample measured at time t after drying at 50 °C in vacuum oven for 60 min and m_i is the initial mass of the sample. At each time point every scaffold was weighed and mechanically tested allowing the degradation pathway of each individual scaffold to be followed with time.

An Arrhenius equation was utilised to extrapolate results at elevated temperatures to physiological temperature [49].

$$k = Ae^{-E_a/RT} \quad (5)$$

where k is reaction rate which will be represented in the current study as the rate of mass loss, A is constant, E_a is the activation energy ($\text{JK}^{-1} \text{mol}^{-1}$), R is universal

gas constant ($\text{JK}^{-1} \text{mol}^{-1}$) and T is the temperature in Kelvin [50].

Mechanical testing

The compressive strength and modulus were determined using a Hounsfield testing machine and the calculations were done according to the standard ASTM 1621-10 : 2010 [51] at 25 ± 1 °C. Scaffolds were inserted vertically between two flat platens of the test machine (load was applied on the cross section). A crosshead speed of 0.5 mm min^{-1} and a 5N load cell was used. The test was carried out up to 20% strain (below the yield strain of the specimens) to obviate permanent deformation within the scaffolds. The measurements were applied on dry samples of $2 \times 4 \times 2$ mm³ dimensions and carried out in three successive cycles with time interval of 10 min to permit scaffold recovery. At various time points the specimens were extracted and dried in vacuum oven at 50 °C for 60 min before testing. Compressive modulus was determined as the gradient of the linear portion of stress-strain curve and strength was determined as the maximum stress at 20% strain.

Optical microscopy

Optical images of LC16 : 4, 18 : 2 and 9 : 1 scaffolds were captured throughout the degradation studies at different temperatures (37, 50 and 65 °C) using a Nikon digital camera (Dxm1200F, Japan) attached to Nikon microscope (Japan). The images were processed using image analysis software (Nikon ACT-1 v. 2.62, LEAD Technologies, USA).

Results and discussion

Material synthesis and evaluation of the writeability

LC is a copolymer constructed from diethylene glycol and two monomers D,L lactide and ϵ -caprolactone. Their relative monomer contents render the polymer more hydrophilic or hydrophobic and influence the degradation rate, viscosity of the precursor and mechanical behavior of the cross-linked and solidified material and degradation behaviour. Starting from the initial composition (LC 18 : 2), two content modifications were synthesized with a) higher ϵ -caprolactone content (LC 16 : 4) and b) shorter chain length (LC 9 : 1). Due to the high viscosity of the lactide-rich modification LC 18 : 2, which negatively effects the processing of the crosslinker, a lactide-rich modification with lower molecular weight (LC 9 : 1) was also synthesized.

The material synthesis method has been described by Davis *et al* [41] for a range of dimethacrylated caprolactone-lactide copolymers with 20 monomer units by tin catalyzed ring-opening polymerization. For TPP, only optical transparent materials are suitable and materials with higher caprolactone contents tending to form optical disturbing crystallites at room temperature. Therefore, lactide-rich varia-

Table 2. Results obtained from 1H-NMR analysis.

	LC 9 : 1	LC 16 : 4	LC 18 : 2
Lactide units	9,6	14,6	19
Caprolactone units	1.3	4.1	2.0
Molecular weight [g mol ⁻¹]	1059	1742	1822
Theoretical (100% yield)	1005	1852	1768
Methacrylation [%]	89.5	88.1	87.4

tions were explored in this study with a LA:CL ratio of 90% (LC 18 : 2) or 80% (LC 16 : 4). In addition, the number of total monomer units added at 90% LA content were halved from 20 units in the LC 18 : 2 to 10 units in LC 9 : 1 to reduce the chain length between the cross-linking methacrylate groups and thus the resulting mesh sizes in the final structure. The results of the synthesis are summarized in table 2 showing correlation with the amounts of educts used, with a deviation of no more than one monomer unit. The lactide richer derivatives (9 : 1 and 18 : 2) tended to incorporate a lactide unit more than the target value, whereas the caprolactone richer LC 16 : 4 had one LA unit less. This also correlated with the molecular weight results obtained for the LC scaffolds, as LC 18 : 2 and 9 : 1 showed higher values (see 3–5%) than theoretical molecular weights, while LC 16 : 4 had 6% less than the predicted value. This was attributed to the fact that the molecular weight of LA was higher than CL (114.14 and 144.13 g mole⁻¹ for CL and LA respectively [52, 53]). The degree of methacrylation was estimated by the integration of the vinyl protons and normalized to the DEG protons at 3.6 ppm which remained unchanged in all variations. High methacrylation (above 85%) was crucial to ensure comparability among the synthesized LC scaffolds throughout the testing. Variation in the methacrylation could lead to less stable structures, more un-solidified residues in the material and open chain ends after photochemical vitrification. This would consequently affect the mechanical properties, cause local acidification and fast degradation of the LC chains due to the lack of complete chain-end-capping with methacrylate groups [54].

For the estimation of the reactivity of the resulting three LC variants a photo-DSC equipped with a UV source was used, allowing insight into the curing behavior of the material prior to the extensive TPP sample preparation (see figure 4). Small values of the time to maximal heat generation t_{\max} correspond to highly reactive photopolymers. Therefore the variants of reactivity in terms t_{\max} were found to be as follows LC 18 : 2 < 16 : 4 < 9 : 1 at 30 °C.

High temperatures foster the curing process expressed by lower t_{\max} values. As clearly shown in figures 4 (A) and (B), LC 18 : 2 was less reactive than LC 9 : 1 and LC 16 : 4 for all temperatures. This was consistent with the generated heat of polymerization. The lower initiation limit of the polymerization with the UV source used appeared to be at 8–9 s, including

the time needed for the lamp to develop full power. LC 9 : 1 generated more heat due to the [molecular weight]:[methacryl-group] ratio, resulting in a higher double bond density which correlated with the higher ΔH values. The temperature dependency was most prominent in LC 9 : 1, resulting in large steps between 30 °C and 70 °C, with a change in ΔH of see 25 J g⁻¹, compared with a change of <8 J g⁻¹ for the other compositions. This could have been related to the higher amount of double bonds present and the accessibility of these with increase in temperature and subsequent reduction in viscosity [55].

For a deeper understanding and better comparison of the three materials, the absolute conversion was calculated equations (2) and (3) (figure 4(C)) [45, 46, 56]. A value of 100% corresponded to complete reaction of the double bonds during network formation upon irradiation; while smaller values corresponded to partially unreacted double bonds and increasing un-solidified phase. The calculations of conversions revealed the high reactivity and large differences between temperatures for LC 9 : 1, which are a result of its incomplete conversion at low temperatures (less than 70%). When rating the different compositions in terms of conversion percentage at 30 °C, they followed the order of LC 16 : 4 > 18 : 2 > 9 : 1. There was no significant difference in t_{\max} of curing for LC 9 : 1 at different temperatures, figure 4. The conversion in LC 9 : 1 appeared to be highly dependent on the temperature. At low temperatures the conversion was the lowest for all precursors, an effect reversed at 70 °C, a temperature at which the motility (molecule size) is a function of conversion. All compositions had potential for structuring using TPP methodology [55].

Manufacturing of 3D scaffolds

The scaffolds were imaged after production in the TPP device to verify consistency of the stereo-lithography (STL) model file with the actual manufactured scaffolds (see figure 5). SEM micrographs revealed a high similarity of structure and consistency with the applied model. The pore sizes for all LC scaffolds were seen 300 μm and throat sizes varied from 152 μm (for LC 9 : 1) to 177 μm (for LC 16 : 4 and 18 : 2), see table 3. Pore geometry deviated from spherical shape to ellipsoidal with aspect ratio of approximately 1.10 for the produced scaffolds. This was suggested to be due to the refractive stretching of the precursor along Z-direction. Pore sizes were in the ideal range of 200–400 μm , known to facilitate osteo-differentiation and functional bone formation [12, 57, 58]. The translation of the STL model to the structure (see figure 5) was good and reproducible in terms of pores and throat sizes achieved (see table 3). Writing parameters were kept constant for all scaffolds since they can influence the mechanical properties and degradation of the resulting polymer structures [59].

SEM was also conducted for investigation of the scaffold microtopography. The surfaces of the scaffolds

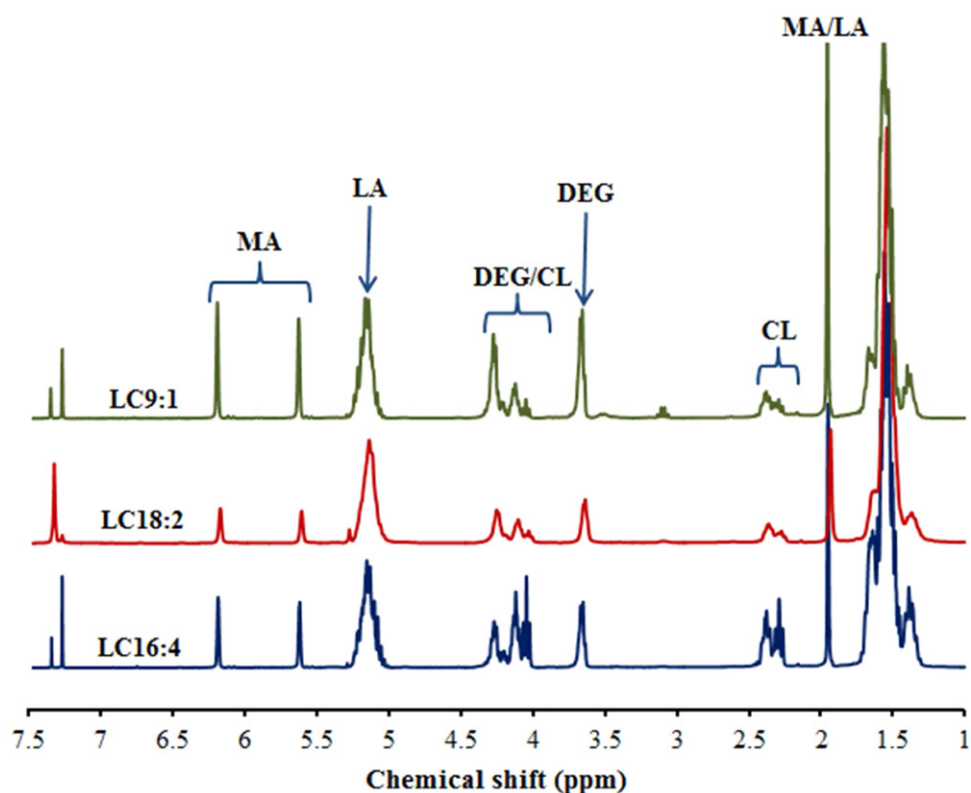


Figure 3. H-NMR spectra of the synthesized materials. The variation is most prominent in the CL signal at 2.5 ppm. DEG: Diethyleneglycol, MA: Methacrylate group, CL: Caprolactone, LA: Lactide.

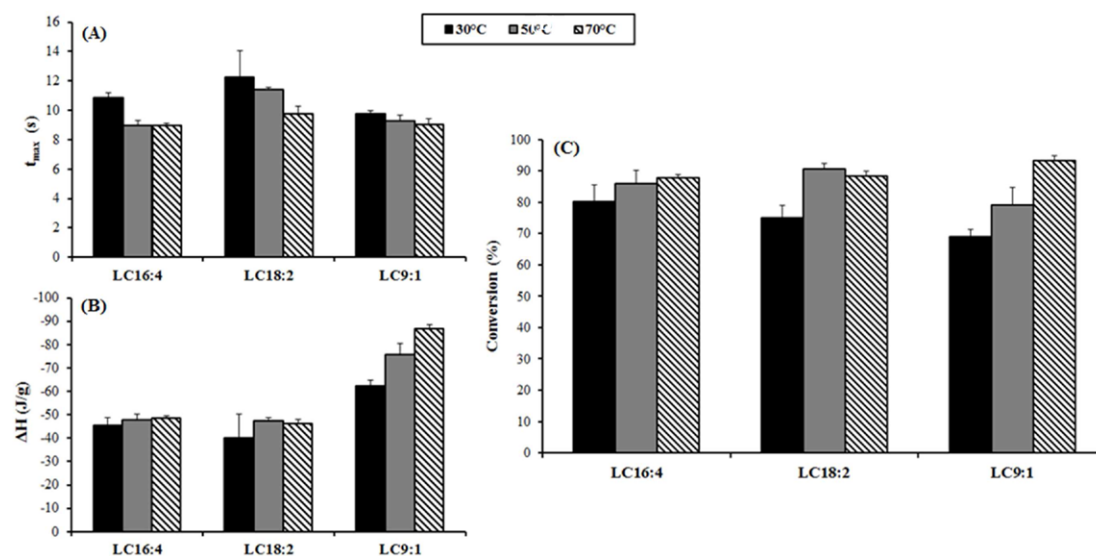


Figure 4. Photo-DSC curing of LC precursor; (A) time of maximal heat generation (t_{max}) of the LC variation at three different temperatures, (B) integrated total heat of reaction (ΔH sample (t)) and (C) absolute conversion of methacrylate groups in LC variants at different temperatures.

had a distinctive texture morphology (see figures 5(B)–(D)), which provided roughness and hence could potentially improve cell adhesion. Figure 5(E) revealed that the line to line distance was visible ($13 \mu\text{m}$), creating room and possibilities for further modification to adhesion and cell preferences. The hatching distance of $13 \mu\text{m}$ was chosen to reduce the writing time and to form pits (see $10 \mu\text{m}$) for physical cellular adhesion.

Scaffold treatment

Since sterilisation is an essential prerequisite for medical devices before use, all the scaffolds were sterilised using gamma radiation at the standard dose of $25 \pm 2.5 \text{ kGy}$ [47, 60] and kept in sterilisation bags prior to use. Gamma radiation was preferred as a method of sterilisation due to its high efficiency, high penetration and negligible thermal effects [61]. However, gamma

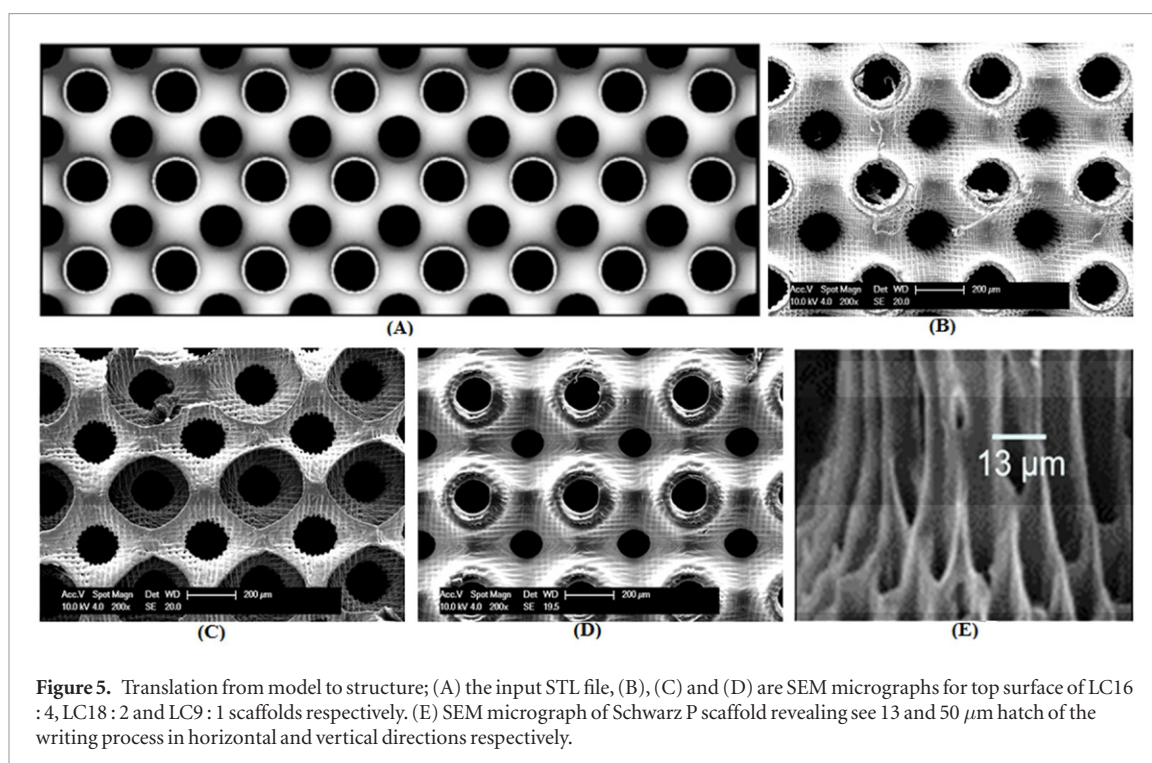


Figure 5. Translation from model to structure; (A) the input STL file, (B), (C) and (D) are SEM micrographs for top surface of LC16 : 4, LC18 : 2 and LC9 : 1 scaffolds respectively. (E) SEM micrograph of Schwarz P scaffold revealing see 13 and 50 μm hatch of the writing process in horizontal and vertical directions respectively.

Table 3. Dimensions of pores, pore throats and aspect ratios of LC scaffolds measured from SEM micrographs.

Scaffold type	Pore size (μm)	Throat size (μm)	Pore aspect ratio
LC16 : 4	314 ± 14	177 ± 7	1.07 ± 0.03
LC18 : 2	328 ± 26	177 ± 10	1.10 ± 0.05
LC9 : 1	290 ± 25	152 ± 7	1.2 ± 0.05

sterilisation is known to induce molecular changes for polymeric materials by chain scission and crosslinking [61–63]. Therefore, the effect of gamma sterilisation on LC scaffolds was also evaluated by compression testing prior to and post sterilisation as shown in figure 6. No significant changes were observed in stress-strain curves for all LC16 : 4, 18 : 2 and 9 : 1 scaffolds post sterilisation. This was suggested to be due to the double effects of gamma irradiation, crosslinking and chain scission, as both have opposite impacts on molecular weight and mechanical properties of the polymers [61–63]. Oliveria *et al* [64] investigated effects of gamma irradiation on molecular weight and tensile properties of poly (3-hydroxybutrate). They found that the molar mass decreased by 80% with the increase of the radiation dose to 25 kGy due to random chain scission. However, no significant changes were observed in tensile strength and modulus up to 25 kGy for the samples presented here.

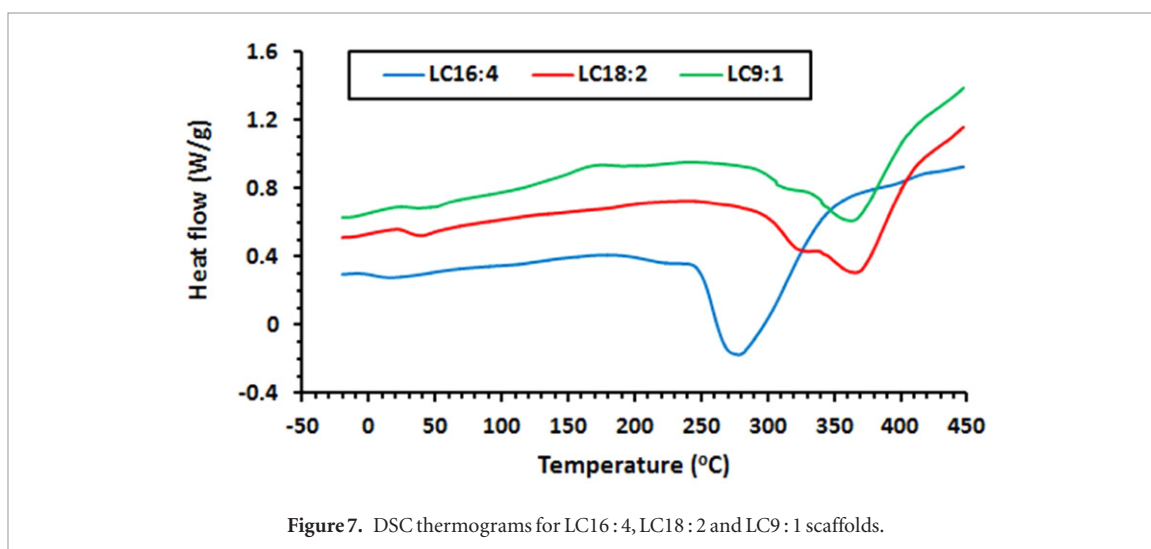
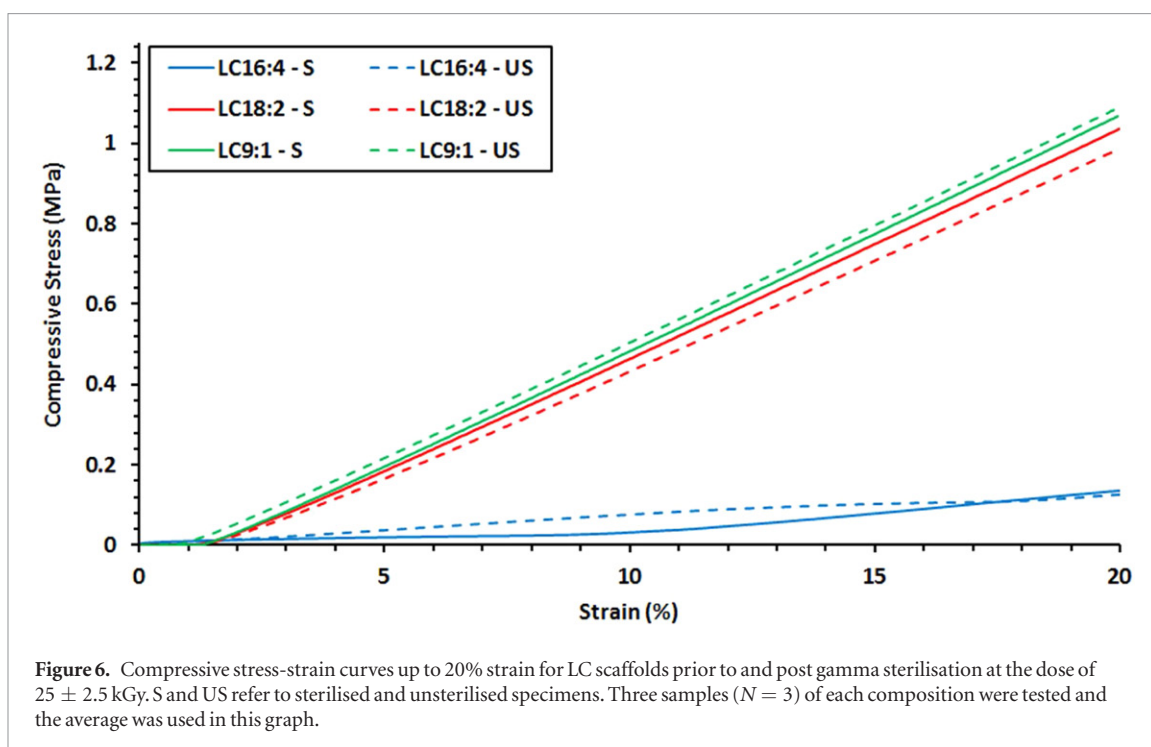
DSC traces for LC scaffolds can be seen in figure 7. The midpoint glass transition temperatures (T_g) for LC16 : 4, 18 : 2 and 9 : 1 were 4.8, 31 and 33 $^{\circ}\text{C}$ respectively. Endothermic peaks were also observed at 281 $^{\circ}\text{C}$ for LC16 : 4 and 365 $^{\circ}\text{C}$ (see figure 7) for LC18 : 2 and 9 : 1, and represented decomposition temperature (T_d). These peaks were suggested to be due to thermal

decomposition of the PLCL copolymers. Values of T_g and T_d for LC18 : 2 and 9 : 1 were similar, whilst LC16 : 4 showed significantly lower results, which was ascribed to the variation in D,L lactide ratio to ϵ -caprolactone (LA/CL) ratio in different scaffolds [65, 66] (see table 2). No crystallisation or melting peaks were detected for any of the scaffolds, possibly due to the high crosslinking in the photo-polymerisation process.

Degradation and mechanical properties

Figures 8 (A)–(C) show changes in weight, mass loss and pH of LC16 : 4, 18 : 2 and 9 : 1 scaffolds versus time throughout degradation in PBS at different temperatures of 37, 50 and 65 $^{\circ}\text{C}$. Initial increases were seen in the wet weight of LC16 : 4, 18 : 2 and 9 : 1 scaffolds respectively up to 5 (at 37 $^{\circ}\text{C}$) and 2 d at 50 and 65 $^{\circ}\text{C}$, followed by stabilisation in weights of all scaffolds. The initial increase was attributed to fast water uptake till specimens attained saturation. LC16 : 4, 18 : 2 and 9 : 1 scaffolds maintained their weight change at ~ 200 , 400 and 250% for the duration of the study at 37 $^{\circ}\text{C}$. This plateau in wet weight of the scaffolds was a result of the balance between water uptake and mass loss [38]. In contrast, a second phase of increase in the scaffold weights was seen after 25 and 6 d of degradation at 50 and 65 $^{\circ}\text{C}$ respectively, which was a consequence of imbalance between water uptake and mass loss (i.e. mass loss due to hydrolytic degradation became dominant) [38].

From figures 8 (D)–(F), the percentage change in mass loss for the scaffolds can be seen versus degradation time at different temperatures. Mass loss for LC16 : 4, 18 : 2 and 9 : 1 scaffolds showed a gradual increase of degradation time at different temperatures. This was attributed to continuous degradation of the scaffold



materials. The relation between percentage of mass loss for all scaffolds and degradation time at 37, 50 and 65 °C followed a linear function with regression coefficient greater than 0.98. Moreover, the rate of mass loss for each scaffold type, determined as the gradient of absolute mass loss versus time, increased as degradation temperature changed from 37 °C to 65 °C. Rates of mass loss of LC16:4 scaffolds at 37, 50 and 65 °C were lower than that for LC18:2 and 9:1. This could be ascribed to the variation in LA/CL ratio between LC16:4, 18:2 and 9:1 scaffold materials (see table 2). It was reported that the required time for complete resorption (degradation time) of poly(D,L-lactide) (PDLA) is approximately 1–2 years, whilst poly(ϵ -caprolactone) (PCL) requires 2–4 years [1, 67, 68]. Consequently, it was expected that an increase in CL content would lead to a lower degradation rate. LC16:4 scaffolds had the highest amount of CL compared to LC18:2 and 9:1 consistent with their

low weight change and mass loss over the degradation in PBS at different temperatures. Note the surface area/volume ratio of the scaffolds depends on pore size and the degradation rate of scaffolds is expected to increase as the surface area/volume ratio increased. However the limited variation in the pore sizes between different LC scaffolds [69, 70] meant these small differences would not influence the degradation effect observed. The degradation and compression tests were completed at day 90 and 83 respectively because the LC18:2 and 9:1 scaffolds became brittle and difficult to handle for weighing and mechanical testing.

The degradation medium (PBS) remained at neutral pH of 7.3 ± 0.1 for all scaffolds during degradation at 37 and 50 °C due to buffering capability of PBS (see figures 8(G) and (H)). At 65 °C, pH of PBS for LC18:2 and 9:1 scaffolds decreased to be around 7.0 after 6 d (see figure 8 I) as a result of faster release of

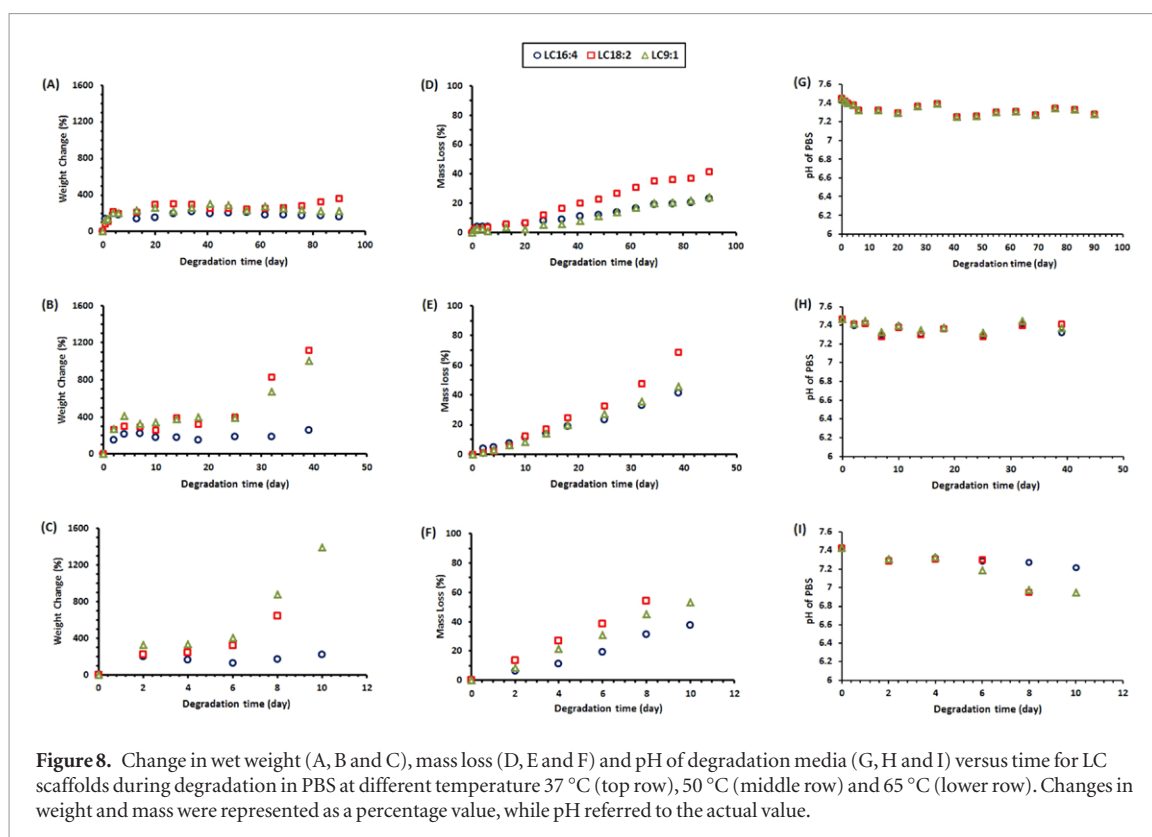


Figure 8. Change in wet weight (A, B and C), mass loss (D, E and F) and pH of degradation media (G, H and I) versus time for LC scaffolds during degradation in PBS at different temperature 37 °C (top row), 50 °C (middle row) and 65 °C (lower row). Changes in weight and mass were represented as a percentage value, while pH referred to the actual value.

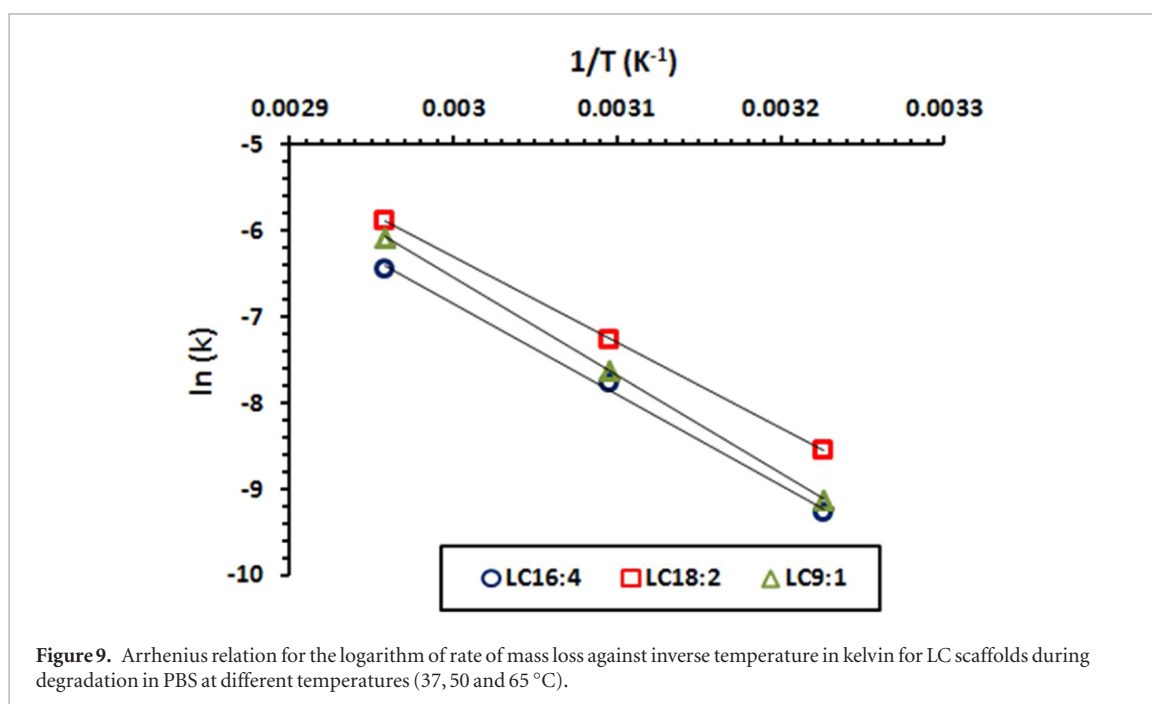


Figure 9. Arrhenius relation for the logarithm of rate of mass loss against inverse temperature in kelvin for LC scaffolds during degradation in PBS at different temperatures (37, 50 and 65 °C).

acidic degradation by-products of poly(L-lactide-co- ϵ -caprolactone).

Calculation of activation energy

The rate of mass loss change for the scaffolds yielded an Arrhenius relationship with regression coefficients greater than 0.99 (see figure 9). The degradation activation energies obtained were 87.9, 82.7 and 94.9 kJ mol^{-1} for LC16 : 4, LC18 : 2 and LC9 : 1 respectively. Arrhenius relation has been conducted for the change in several parameters of biodegradable polymers such

as molecular weight, breaking strength, viscosity and mass loss [34, 38, 49, 71, 72]. The majority of previous publications used change in molecular weight over degradation time at different temperatures. However, it was not applicable to measure the molecular weight for photo cross-linked copolymers using gel permeation chromatography (GPC) due to their insolubility in organic solvents. Therefore, the change in rate of mass loss at different temperatures was used in this study to calculate the degradation activation energy. Weir *et al* [49] and Agrawal *et al* [71] determined activation

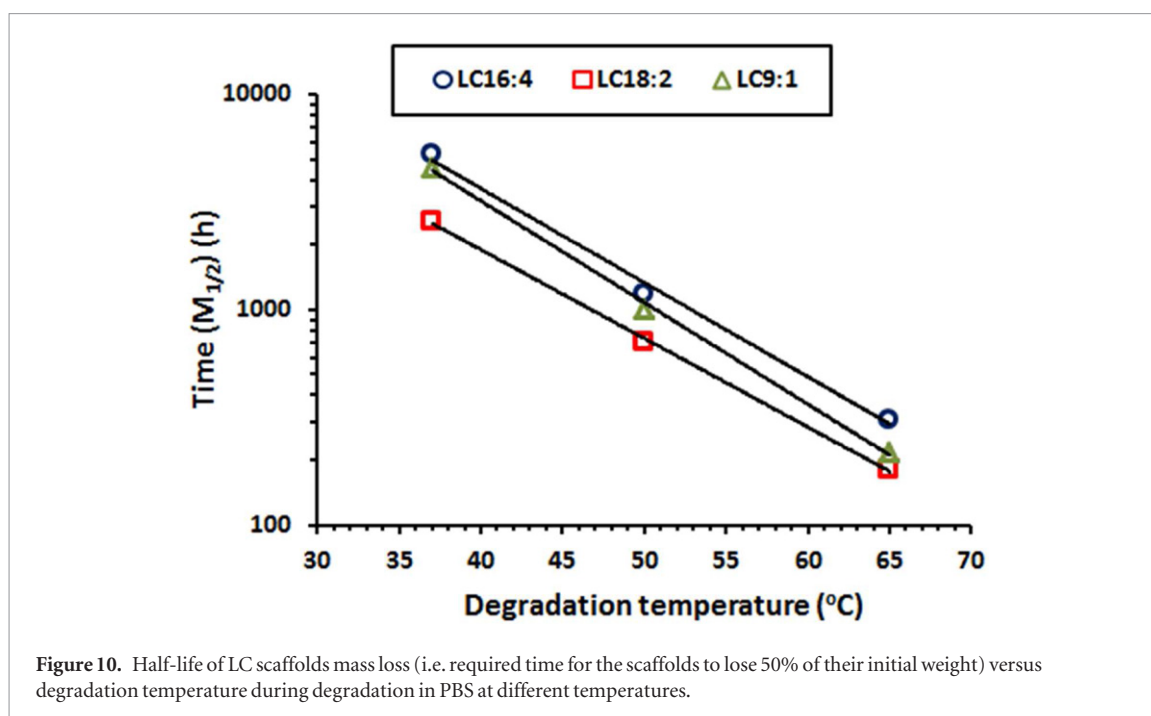


Figure 10. Half-life of LC scaffolds mass loss (i.e. required time for the scaffolds to lose 50% of their initial weight) versus degradation temperature during degradation in PBS at different temperatures.

energies for 50%PLA-50%PGA copolymer and PLLA (113.9 and 100.5 kJ mol⁻¹) through the change in molecular weight against degradation temperature. Degradation activation energy was also determined for 10%PLLA-90%PGA through change in tensile breaking strength during degradation at different temperatures [40]. The activation energy ranged between 95.9 kJ mol⁻¹ and 102.6 kJ mol⁻¹. Pietrzak *et al* [34] applied the Arrhenius equation to change in inherent viscosity for a 82%PLLA-18%PGA copolymer and obtained an activation energy of 100.1 kJ mol⁻¹. Previous studies have suggested that degradation activation energies were independent of the geometry and composition of the PLLA-PGA copolymers. The values of activation energy obtained for LC scaffolds using rate of mass loss were similar to the published results for biodegradable polymers [34, 40, 71].

Prediction of long-term effects

A correlation between a long-term degradation study at 37 °C and short studies at elevated temperatures (50 and 65 °C) was conducted in order to make a prediction for degradation time, using a similar procedure to that presented by Litherland *et al* [73]. By fitting plots relating half-life of mass loss (Time (M_{1/2})), required time for the scaffold to lose 50% of their initial weight, to degradation temperature, a power equation were obtained (see figure 10) and regression coefficients were greater than 0.99. Therefore, the degradation rate of the scaffolds at other degradation temperatures could be anticipated through the obtained fitting equations.

The changes in compressive modulus and strength of LC16 : 4, 18 : 2 and 9 : 1 scaffolds against time during degradation in PBS at 37 °C are shown in figure 11. Before degradation, compressive moduli were 0.27, 2 and 4 MPa for LC16 : 4, 18 : 2 and 9 : 2 respectively. Compressive strengths at 20% strain for LC18 : 2 and 9

: 1 (0.2 and 0.55 MPa) scaffolds were also significantly higher ($P < 0.001$) than LC16 : 4 (0.05 MPa). Mechanical properties of these scaffolds were mainly dependent on their material composition (i.e. LA/CL ratio) as all scaffolds have almost the same porosity and pore sizes. Young's modulus for poly(D,L-lactide) is approximately five times higher than poly(ϵ -caprolactone) alone [67, 68]. Therefore, mechanical properties of the copolymer would be expected to decrease as the CL content increased as shown in figure 11. Similar findings were published for poly(L-lactide-co- ϵ -caprolactone) copolymers by Fernandez *et al* [66]. Tensile modulus and strength of the copolymer films decreased from 1343 to 12 MPa and from 26.6 to 17.2 MPa respectively as the CL contents increased from 10 to 30%. No significant changes ($P > 0.05$) were seen in both strength and modulus for all scaffolds over 20 d of degradation in PBS at 37 °C. After this period all scaffolds showed decreases in strength and modulus till end of the study at 83 d. The large errors for LC18 : 2 and 9 : 1 scaffolds were due to the mechanical testing temperature (25 ± 1 °C) which unfortunately was close to the onset glass transition temperature for LC18 : 2 and 9 : 1 (23.7 ± 0.7 °C). The onset glass transition for LC16 : 4 scaffolds (-1.6 ± 1 °C) was significantly lower than the testing temperature and this explained the lower variation in results showing a smooth and gradual decrease in their compressive modulus and strength properties (inset, figures 11 (A) and (B)). Reduction in compressive properties for all scaffolds over time was ascribed to continuous degradation of the scaffold materials as can be seen from variations in mass loss against time (see figure 8(D)).

Temperature and strain conditions (25 °C and 20% respectively) of compressive testing were chosen to fit the surgical environment and handling procedures. Temperature of the surgery theatre is usually fixed at 25 °C

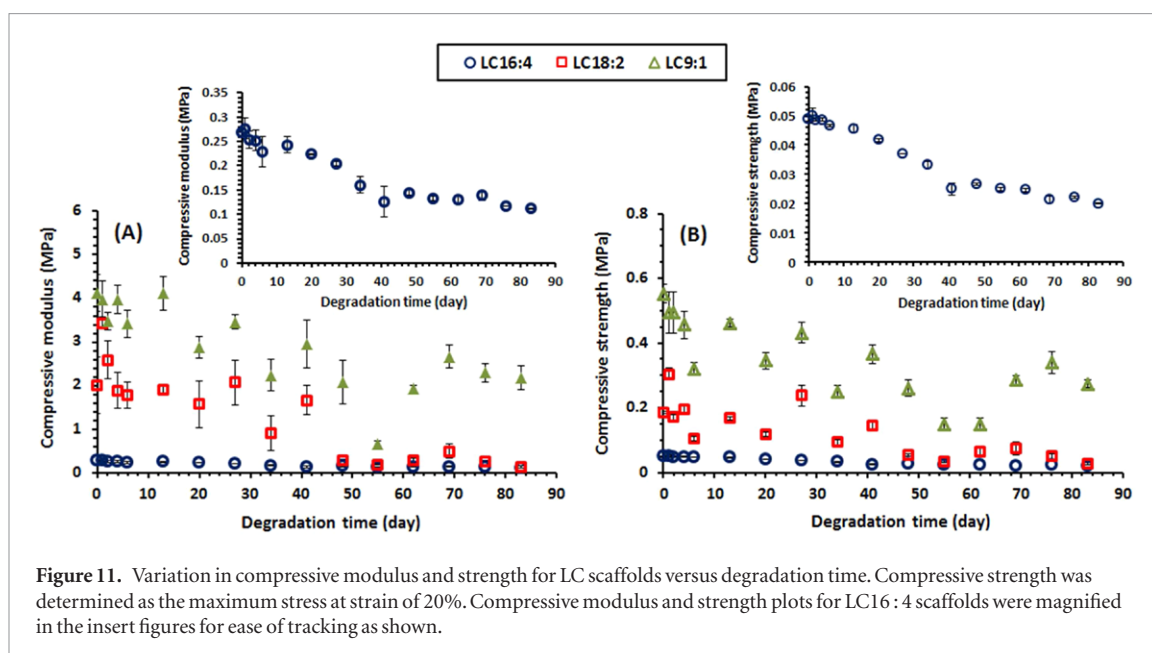


Figure 11. Variation in compressive modulus and strength for LC scaffolds versus degradation time. Compressive strength was determined as the maximum stress at strain of 20%. Compressive modulus and strength plots for LC16 : 4 scaffolds were magnified in the insert figures for ease of tracking as shown.

and the surgeon is anticipated to compress the scaffold up to 20% before implantation in order to obviate scaffold dislocation.

For LC16 : 4 scaffolds, no significant visual changes were detected at different time points and temperatures. Conversely, large deteriorations were observed for LC18 : 2 and 9 : 1 scaffolds in particular at elevated temperatures. This was due to two reasons; fast degradation rates and thermal effects. Repeatable heating-cooling cycles during degradation at 37 °C and testing or changing PBS at room temperature (~20 °C) were suggested to accelerate the degradation rate of the scaffolds (thermal effect). Effects of heating-cooling cycles were more significant on LC18 : 2 and 9 : 1 than LC16 : 4 due to their thermal properties (see figure 7). Heating-cooling cycles covered a range of temperatures (37 °C–20 °C) which was around their glass transition temperature for LC18 : 2 and 9 : 1 scaffolds, whilst T_g of LC16 : 4 was out of this range.

Conclusions

Three dimensional porous scaffolds were manufactured via a TPP technology based on a Schwarz Primitive minimal surface derived unit cells with μm resolution and pore size of about 300 μm . For commercialization, the writing time is still the main limitation, for example for manufacturing scaffolds of one cubic centimeter with the current set-up would lead to writing times of see 6 d. Nevertheless the technology is constantly improving and recent approaches managed to create scaffolds bigger than 15 mm^3 [74, 75] and offer encouraging preclinical results [76] underlining the potential of TPP to deliver microstructures of good reproducibility at scale. Changes in thermal, degradation and mechanical properties of all scaffolds were related to their chemical composition (LA/CL ratio) and accelerated degradation was predictable as the rate of mass loss for all scaffolds increased

gradually by increasing degradation temperature from 37 to 65 °C. The activation energies for degradation were independent of chain length and composition. By applying a temperature superposition, a feasible accelerated method was generated to predict long-term degradation time for LC scaffolds at 37 °C. These materials have the potential to replace state-of-the-art implants and allografts as they can offer slower degradation and softer mechanics and avoid the acidity-burst at degradation compared to LA, and they will be translated into biological testing to determine the effect of CL on osteogenesis.

Acknowledgments

This research project has received funding from the European Union's Seventh Framework Programme (FP7/2007–2013) under grant agreement no. 263363

References

- [1] Woodruff MA and Hutmacher DW 2010 The return of a forgotten polymer—Polycaprolactone in the 21st century *Prog. Polym. Sci.* **35** 1217–56
- [2] Woodruff MA, Lange C, Reichert J, Berner A, Chen F, Fratzl P, Schantz J-T and Hutmacher DW 2012 Bone tissue engineering: from bench to bedside *Mater. Today* **15** 430–5
- [3] Ulery B D, Nair L S and Laurencin C T 2011 Biomedical applications of biodegradable polymers *J. Polym. Sci. B* **49** 832–64
- [4] Yang X B, Bhatnagar R S, Li S and Oreffo R O 2004 Biomimetic collagen scaffolds for human bone cell growth and differentiation *Tissue Eng.* **10** 1148–59
- [5] Ho M-H, Kuo P-Y, Hsieh H-J, Hsien T-Y, Hou L-T, Lai J-Y and Wang D-M 2004 Preparation of porous scaffolds by using freeze-extraction and freeze-gelation methods *Biomaterials* **25** 129–38
- [6] Lannutti J, Reneker D, Ma T, Tomasko D and Farson D 2007 Electrospinning for tissue engineering scaffolds *Mater. Sci. Eng. C* **27** 504–9
- [7] Brown T D, Edin F, Detta N, Skelton A D, Hutmacher D W and Dalton P D 2014 Melt electrospinning of poly(epsilon-caprolactone) scaffolds: phenomenological observations

AQ1

AQ2

AQ3

- associated with collection and direct writing *Mater. Sci. Eng. C* **45** 698–708
- [8] Brown T D, Dalton P D and Huttmacher D W 2011 Direct writing by way of melt electrospinning *Adv. Mater.* **23** 5651–7
- [9] Zhu J 2010 Bioactive modification of poly(ethylene glycol) hydrogels for tissue engineering *Biomaterials* **31** 4639–56
- [10] Lutolf M P and Hubbell J A 2005 Synthetic biomaterials as instructive extracellular microenvironments for morphogenesis in tissue engineering *Nat. Biotechnol.* **23** 47–55
- [11] Tsang V L and Bhatia S N 2004 3D tissue fabrication *Adv. Drug Deliv. Rev.* **56** 1635–47
- [12] Tse J R and Engler A J 2010 Preparation of hydrogel substrates with tunable mechanical properties *Curr. Protoc. Cell Biol.* / editorial board, Juan S. Bonifacino ... [et al.] **Chapter 10**: p. Unit 10 16
- [13] Huttmacher D W 2000 Scaffolds in tissue engineering bone and cartilage *Biomaterials* **21** 2529–43
- [14] Landers R, Hubner U, Schmelzeisen R and Mulhaupt R 2002 Rapid prototyping of scaffolds derived from thermoreversible hydrogels and tailored for applications in tissue engineering *Biomaterials* **23** 4437–47
- [15] Rentsch B, Bernhardt R, Scharnweber D, Schneiders W, Rammelt S and Rentsch C 2012 Embroidered and surface coated polycaprolactone-co-lactide scaffolds: a potential graft for bone tissue engineering *Biomater.* **2** 158–65
- [16] Stampf J, Baudis S, Heller C, Liska R, Neumeister A, Kling R, Ostendorf A and Spitzbart M 2008 Photopolymers with tunable mechanical properties processed by laser-based high-resolution stereolithography *J. Micromech. Microeng.* **18** 125014
- [17] Lee K-W, Wang S, Fox B C, Ritman E L, Yaszemski M J and Lu L 2007 Poly(propylene fumarate) bone tissue engineering scaffold fabrication using stereolithography: effects of resin formulations and laser parameters *Biomacromolecules* **8** 1077–84
- [18] Sugioka K and Cheng Y 2014 Ultrafast lasers [mdash] reliable tools for advanced materials processing *Light Sci. Appl.* **3** e149
- [19] Malinauskas M, Farsari M, Piskarskas A and Juodkazis S 2013 Ultrafast laser nanostructuring of photopolymers: a decade of advances *Phys. Rep.* **533** 1–31
- [20] Maruo S and Fourkas J T 2008 Recent progress in multiphoton microfabrication *Laser Photon. Rev.* **2** 100–11
- [21] Malinauskas M, Purlys V, Rutkauskas M, Gaidukevičiūtė A and Gadonas R 2010 Femtosecond visible light induced two-photon photopolymerization for 3D micro/nanostructuring in photoresists and photopolymers *Lithuanian J. Phys.* **50** 201–7
- [22] Malinauskas M, Danilevičius P and Juodkazis S 2011 3D micro-/nano-structuring via direct write polymerization with picosecond laser pulses *Opt. Express* **19** 5602–10
- [23] Galajda P and Ormos P 2001 Complex micromachines produced and driven by light *Appl. Phys. Lett.* **78** 249–51
- [24] Kawata S, Sun H-B, Tanaka T and Takada K 2001 Finer features for functional microdevices *Nature* **412** 697–8
- [25] Weiß T, Schade R, Laube T, Berg A, Hildebrand G, Wyrwa R, Schnabelrauch M and Liefelth K 2011 Two-photon polymerization of biocompatible photopolymers for microstructured 3D biointerfaces *Adv. Eng. Mater.* **13** B264–73
- [26] Berg A, Wyrwa R, Weisser J, Weiss T, Schade R, Hildebrand G, Liefelth K, Schneider B, Ellinger R and Schnabelrauch M 2011 Synthesis of photopolymerizable hydrophilic macromers and evaluation of their applicability as reactive resin components for the fabrication of three-dimensionally structured hydrogel matrices by 2-photon-polymerization *Adv. Eng. Mater.* **13** B274–84
- [27] Weiss Y T, Hildebrand G, Schade R and Liefelth K 2009 Two-Photon polymerization for microfabrication of 3D scaffolds for tissue engineering application *Eng. Life Sci.* **9** 384–90
- [28] Danilevičius P, Georgiadi L, Pateman C J, Claeysens F, Chatzinikolaïdou M and Farsari M 2015 The effect of porosity on cell ingrowth into accurately defined, laser-made, polylactide-based 3D scaffolds *Appl. Surf. Sci.* **336** 2–10
- [29] Claeysens F *et al* 2009 3D Biodegradable Structures Fabricated by Two-Photon Polymerization *Langmuir* **25** 3219–23
- [30] Ovsianikov A, Malinauskas M, Schlie S, Chichkov B, Gittard S, Narayan R, Löbner M, Sternberg K, Schmitz K P and Haverich A 2011 3D laser micro- and nano-structuring of acrylated poly(ethylene glycol) materials and evaluation of their cytotoxicity for tissue engineering applications *Acta Biomater.* **7** 967–74
- [31] Da Sie Y, Li Y-C, Chang N-S, Campagnola P J and Chen S-J 2015 Fabrication of 3D multi-protein microstructures for cell migration and adhesion enhancement *Biomed. Opt. Express* **6** 480–90
- [32] Turunen S, Käpylä E, Terzaki K, Viitanen J, Fotakis C, Kellomäki M and Farsari M 2011 Pico- and femtosecond laser-induced crosslinking of protein microstructures: evaluation of processability and bioactivity *Biofabrication* **3** 045002
- [33] Justinas M *et al* 2015 Preclinical study of SZ2080 material 3D microstructured scaffolds for cartilage tissue engineering made by femtosecond direct laser writing lithography *Biofabrication* **7** 015015
- [34] Pietrzak W S, Kumar M and Eppley B L 2003 The influence of temperature on the degradation rate of lactosorb copolymer *J. Craniofac. Surg.* **14** 176–83
- [35] Lam C X, Savalani M M, Teoh S H and Huttmacher D W 2008 Dynamics of *in vitro* polymer degradation of polycaprolactone-based scaffolds: accelerated versus simulated physiological conditions *Biomed. Mater.* **3** 034108
- [36] Lee S-H, Lee J and Cho Y-S 2014 Analysis of degradation rate for dimensionless surface area of well-interconnected PCL scaffold via *in vitro* accelerated degradation experiment *Tissue Eng. Regen. Med.* **11** 446–52
- [37] Lyu S, Schley J, Loy B, Lind D, Hobot C, Sparer R and Untereker D 2007 Kinetics and time-temperature equivalence of polymer degradation *Biomacromolecules* **8** 2301–10
- [38] Felfel R M, Hossain K M Z, Parsons A J, Rudd C D and Ahmed I 2015 Accelerated *in vitro* degradation properties of poly(lactic acid)/phosphate glass fibre composites *J. Mater. Sci.* **50** 3942–55
- [39] Claes L E, Ignatius A A, Rehm K E and Scholz C 1996 New bioresorbable pin for the reduction of small bony fragments: design, mechanical properties and *in vitro* degradation *Biomaterials* **17** 1621–6
- [40] Deng M, Zhou J, Chen G, Burkley D, Xu Y, Jamiolkowski D and Barbolt T 2005 Effect of load and temperature on *in vitro* degradation of poly(glycolide-co-L-lactide) multifilament braids *Biomaterials* **26** 4327–36
- [41] Davis K A, Burdick J A and Anseth K S 2003 Photoinitiated crosslinked degradable copolymer networks for tissue engineering applications *Biomaterials* **24** 2485–95
- [42] Wang S, Lu L, Gruetzmacher J A, Currier B L and Yaszemski M J 2006 Synthesis and characterizations of biodegradable and crosslinkable poly(ϵ -caprolactone fumarate), poly(ethylene glycol fumarate), and their amphiphilic copolymer *Biomaterials* **27** 832–41
- [43] Cai L and Wang S 2010 Elucidating colorization in the functionalization of hydroxyl-containing polymers using unsaturated anhydrides/acyl chlorides in the presence of triethylamine *Biomacromolecules* **11** 304–7
- [44] Cai L and Wang S 2010 Poly(ϵ -caprolactone) acrylates synthesized using a facile method for fabricating networks to achieve controllable physicochemical properties and tunable cell responses *Polymer* **51** 164–77
- [45] Wu K C and Halloran J W 2005 Photopolymerization monitoring of ceramic stereolithography resins by FTIR methods *J. Mater. Sci.* **40** 71–6
- [46] Lovestead T M, Burdick J A, Anseth K S and Bowman C N 2005 Understanding multivinyl monomer photopolymerization kinetics through modeling and GPC investigation of degradable networks *Polymer* **46** 6226–34
- [47] BS EN ISO 11137-2 (2013) *Sterilization of Health care Products. Radiation. Establishing the Sterilization Dose*
- [48] 10993-13, B.E.I 2010 *Biological Evaluation of Medical Devices. Identification and Quantification of Degradation Products From Polymeric Medical Devices*

AQ4

- [49] Weir N, Buchanan F, Orr J, Farrar D and Dickson G 2004 Degradation of poly-L-lactide. Part 2: increased temperature accelerated degradation *Proc. Inst. Mech. Eng. H* **218** 321–30
- [50] Weir N, Buchanan F, Orr J and Dickson G 2004 Degradation of poly-L-lactide. Part 1: *in vitro* and *in vivo* physiological temperature degradation *Proc. Inst. Mech. Eng. H* **218** 307–19
- [51] ASTM D1621—10 2010 *Standard Test Method for Compressive Properties of Rigid Cellular Plastics*
- [52] Li C-Y, Liu D-C and Ko B-T 2013 Synthesis, characterization and reactivity of single-site aluminium amides bearing benzotriazole phenoxide ligands: catalysis for ring-opening polymerization of lactide and carbon dioxide/propylene oxide coupling *Dalton Trans.* **42** 11488–96
- [53] Heijkants R G J C, Schwab L W, van Calck R V, de Groot J H, Pennings A J and Schouten A J 2005 Extruder synthesis of a new class of polyurethanes: Polyacylurethanes based on poly(ϵ -caprolactone) oligomers *Polymer* **46** 8981–9
- [54] Burdick J A, Frankel D, Dernel W S and Anseth K S 2003 An initial investigation of photocurable 3D lactic acid based scaffolds in a critical-sized cranial defect *Biomaterials* **24** 1613–20
- [55] Tobita H 1998 Molecular weight distribution formed through chain-length-dependent crosslinking reactions *Macromol. Theory Simul.* **7** 225–32
- [56] Ye Q, Spencer P, Wang Y and Misra A 2007 Relationship of solvent to the photopolymerization process, properties, and structure in model dentin adhesives *J. Biomed. Mater. Res. A* **80** 342–50
- [57] Papaioannou T G, Karatzis E N, Vavuranakis M, Lekakis J P and Stefanadis C 2006 Assessment of vascular wall shear stress and implications for atherosclerotic disease *Int. J. Cardiol.* **113** 12–8
- [58] Papaioannou T G and Stefanadis C 2005 Vascular wall shear stress: basic principles and methods *Hellenic J. Cardiol.* **46** 9–15
- [59] Farkas B, Romano I, Ceseraciu L, Diaspro A, Brandi F and Beke S 2015 Four-order stiffness variation of laser-fabricated photopolymer biodegradable scaffolds by laser parameter modulation *Mater. Sci. Eng. C* **55** 14–21
- [60] Kowalski J B, Aoshuang Y and Tallentire A 2000 Radiation sterilization — evaluation of a new approach for substantiation of 25 kGy *Radiat. Phys. Chem.* **58** 77–86
- [61] Cottam E, Hukins D W L, Lee K, Hewitt C and Jenkins M J 2009 Effect of sterilisation by gamma irradiation on the ability of polycaprolactone (PCL) to act as a scaffold material *Med. Eng. Phys.* **31** 221–6
- [62] Narkis M, Sibony-Chaouat S, Siegmann A, Shkolnik S and Bell J P 1985 Irradiation effects on polycaprolactone *Polymer* **26** 50–4
- [63] Augustine R, Saha A, Jayachandran V P, Thomas S and Kalarikkal N 2015 Dose-Dependent effects of gamma irradiation on the materials properties and cell proliferation of electrospun polycaprolactone tissue engineering scaffolds *Int. J. Polym. Mater. Polym. Biomater.* **64** 526–33
- [64] Oliveira L M, Araujo P L B and Araujo E S 2013 The effect of gamma radiation on mechanical properties of biodegradable polymers poly(3-hydroxybutyrate) and poly(3-hydroxybutyrate-co-3-hydroxyvalerate) *Mater. Res.* **16** 195–203
- [65] Fernández J, Larrañaga A, Etxeberria A, Wang W and Sarasua J R 2013 A new generation of poly(lactide/ ϵ -caprolactone) polymeric biomaterials for application in the medical field *J. Biomed. Mater. Res. A* **102** 3573–84
- [66] Fernández J, Etxeberria A and Sarasua J-R 2012 Synthesis, structure and properties of poly(L-lactide-co--caprolactone) statistical copolymers *J. Mech. Behav. Biomed. Mater.* **9** 100–12
- [67] Middleton J C and Tipton A J 2000 Synthetic biodegradable polymers as orthopedic devices *Biomaterials* **21** 2335–46
- [68] Maurus P B and Kaeding C C 2004 Bioabsorbable implant material review *Oper. Tech. Sports Med.* **12** 158–60
- [69] Sung H-J, Meredith C, Johnson C and Galis Z S 2004 The effect of scaffold degradation rate on 3D cell growth and angiogenesis *Biomaterials* **25** 5735–42
- [70] Yang S, Leong K F, Du Z and Chua C K 2001 The design of scaffolds for use in tissue engineering. Part I. Traditional factors *Tissue Eng.* **7** 679–89
- [71] Agrawal C M, Huang D, Schmitz J P and Athanasiou K A 1997 Elevated temperature degradation of a 50:50 copolymer of PLA-PGA *Tissue Eng.* **3** 345–52
- [72] Deng M, Chen G, Burkley D, Zhou J, Jamiolkowski D, Xu Y and Vetrecin R 2008 A study on *in vitro* degradation behavior of a poly(glycolide-co-l-lactide) monofilament *Acta Biomater.* **4** 1382–91
- [73] Litherland K L, Oakley D R and Proctor B A 1981 The use of accelerated ageing procedures to predict the long term strength of GRC composites *Cement Concr. Res.* **11** 455–66
- [74] Hsieh T M, Benjamin Ng C W, Narayanan K, Wan A C A and Ying J Y 2010 3D microstructured tissue scaffolds fabricated by two-photon laser scanning photolithography *Biomaterials* **31** 7648–52
- [75] Ovsianikov A, Mironov V, Stampfl J and Liska R 2012 Engineering 3D cell-culture matrices: multiphoton processing technologies for biological and tissue engineering applications *Expert Rev. Med. Devices* **9** 613–33
- [76] Bückmann T, Thiel M, Kadic M, Schittny R and Wegener M 2014 An elasto-mechanical unfeelability cloak made of pentamode metamaterials *Nat. Commun.* **5**

QUERIES

Page 12

AQ1

We have been provided funding information for this article as below. Please confirm whether this information is correct. European Union's Seventh Framework Programme: 263363.

Page 12

AQ2

Please check the details for any journal references that do not have a link as they may contain some incorrect information.

Page 13

AQ3

Please provide the volume and page/article number for reference [12].

AQ4

Publisher location and names are required for all book references. Please provide the missing information for references [47, 48, 51]

Page 14

AQ5

Please provide the page/article number for reference [76].